Progress In Electromagnetics Research C, Vol. 127, 127–143, 2022

Inkjet Printed Flexible High Isolation Patch Antenna for 5.8 GHz Full-Duplex Applications

Abdul R. Hossain[1, *], Md S. I. Sagar[1], Nghi Tran[2], Praveen K. Sekhar[1], and Tutku Karacolak[1]

Abstract—In this paper, a flexible full-duplex antenna is proposed with robust performance and high isolation for 5.8 GHz using foam and PET paper. The patch of the antenna is modified by corner cut and inset feeding, while the defected ground structure is used to improve isolation between transmit and receive ports. Silver nanoparticle ink is used for printing the antenna in an inkjet printer. The fabricated version supports simulated results by showing acceptable performance in desired bandwidth. Bending tests and human body loading experiments are carried out on the fabricated antenna to demonstrate antenna's effectiveness for wearable applications. To the best of authors' knowledge, this is the first flexible full-duplex antenna designed, achieving a high isolation level of −50 dB. Moreover, wide bandwidth, improved gain, radiation efficiency, low cost, easy fabrication, and robust performance make it a good option for 5.8 GHz wearable applications.

1. INTRODUCTION

With the increase in the number of devices getting connected to the internet network, 5 GHz WiFi band, which is more precisely from 5.725 GHz to 5.875 GHz, having a center frequency of 5.8 GHz, needs to be utilized more to prevent 2.4 GHz band from getting saturated. Moreover, implementing a full-duplex antenna will double the spectral efficiency [1]. Full-duplex transmission mode transmits and receives signals simultaneously in the same frequency band, making the number of devices used in the band twice and hence improving the spectral efficiency to double. However, full-duplex mode needs around −100 dB isolation between transmitting and receiving signals. This −100 dB isolation can be achieved with combined efforts in antenna, analog circuits, and digital signal processing. Achieving isolation around −50 dB in antenna level helps to design other levels with less complexity and reduced cost.

Researchers have designed and characterized full-duplex antennas on different materials targeting different frequency ranges. In [2], a full-duplex antenna is proposed on an FR4 epoxy substrate with a ring hybrid feeding structure and a T-shaped defected ground structure (DGS) at 2.4 GHz. An antenna array is proposed in [3] with a slotline based 180° hybrid structure to improve isolation to −50 dB at 4.75 GHz to 5.18 GHz. In [4], a broadband dual polarized metasurface based antenna is proposed to operate at 3.5 GHz for in band full-duplex applications, where differential feeding scheme is applied to create high isolation. However, all of these antennas are on rigid materials meaning that they are not suitable for flexible and wearable applications.

Recently, next generation devices are getting flexible in nature because of advantages like light weight, cheapness, portability, and durability. Thus, the demand for flexible antennas is increasing as it is one of the most essential elements for the flexible device. Materials like polyethylene terephthalate (PET), polyethersulphone (PES), polycarbonate (PC), polyimide (PI), polyethylene

Received 14 October 2022, Accepted 24 November 2022, Scheduled 3 December 2022

* Corresponding author: Abdul Rakib Hossain (abdul.hossain@wsu.edu).

[1] School of Engineering and Computer Science, Washington State University Vancouver, Washington, USA. [2] Department of Electrical and Computer Engineering, University of Akron, Ohio, USA.

naphthalate (PEN), and polydimethylsiloxane (PDMS) are used as substrates for flexible antennas [5]. Textile based antenna is also getting much attention as it is a promising option for wearable antennas [6–8]. Inkjet printing [9], 3-D printing [10], screen printing [11], and chemical etching [12] are popular methods for the antenna fabrication on polymer substrates, whereas stitching and embroidery [13] are used for textile antennas.

Flexible antennas working at 5.8 GHz are studied widely using different materials and printing processes. In [14], a microstrip-fed slot antenna is proposed for 5.3 GHz–6.3 GHz using PEDOT:PSS conductive polymer. A dual-band CPW-fed antenna working in 2.44 GHz and 5.8 GHz bands using flexible Rogers Ultralam 3850 is proposed in [15]. Another dual-band antenna is designed on denim material which works on 2.45 GHz and 5.8 GHz [16]. A wide band antenna working from 1 GHz to 8 GHz is proposed in [17] using a kapton substrate. In another recent work [18], an ultra-wideband antenna operating from 5.2 GHz to 41 GHz is proposed, which is fabricated on liquid crystal polymer (LCP). However, none of these antennas have full-duplex capacity. In [19], a textile antenna is proposed for 2.4 GHz full-duplex wearable applications, where two additional strips are placed perpendicularly to the feed lines for improving bandwidth and isolation between ports. This work has reported −20 dB isolation, which is not very effective in full-duplex systems due to low isolation. Similarly, in [20] and [21] dual-polarized antennas are proposed for on-/off-body wearable applications. Both designs demonstrate low isolation values between TX and RX ports, making them not suitable for full-duplex systems. Another work [22] proposes a substrate integrated waveguide (SIW) based antenna operating at 4.8 GHz and 5.8 GHz with an isolation level of −29.8 dB for wearable applications. However, this antenna also lacks the necessary level of isolation as well as a more complex fabrication process than other candidates.

In this article, an inkjet printed full-duplex flexible antenna on PET substrate is proposed, which will work on 5.8 GHz and can be effectively used for flexible and wearable applications. The main contribution of this work is the proposal of a full-duplex antenna at 5.8 GHz, as this will be one of the most used frequency bands in the near future. The proposed antenna shows the measured high isolation of −68 dB in 5.8 GHz while maintaining a −10 dB bandwidth from 5.66 GHz to 5.95 GHz. Also, presenting it as a flexible device enhances its arena of applications. Simulation and experimental studies are carried out to show the effectiveness of the antenna for bending situations and human tissue loading. This antenna ushers the domain of designing flexible full-duplex antenna. To the best of our knowledge, this design has the highest isolation achieved for flexible full-duplex systems. This work is an improvement and extension of the authors' previous work [23]. The design in [23] has lower bandwidth and lower isolation with shifted resonance frequency from 5.8 GHz. It is based on simulation results without fabrication and validation of the antenna model. In addition to improved performance, the current work presents measured results, bending tests, on body characterization, human phantom loading analysis, specific absorption rate (SAR) analysis, and a detailed discussion of the design process.

This article is organized as follows. Section 2 describes the proposed design, design steps, and the effect of human phantom loading mainly. Section 3 details the fabrication process of the antenna, measured results, and bending characteristics, followed by a conclusion in Section 4.

2. ANTENNA DESIGN

2.1. Design Configuration

The proposed flexible antenna consists of three layers. Top and bottom layers are PET paper, and middle layer is foam. Each PET paper layer has a thickness of 0.135 mm, and the foam layer has a thickness of 1.6 mm. The relative permittivity of the PET paper is 3.2, and the loss tangent is 0.022. Commercially available low loss flexible foam from Cuming Microwave is used here, with a relative permittivity of 1.06 and a loss tangent of 0.0001. The length and width of the proposed antenna are 42 mm and 125 mm, respectively. In the top layer, two patches are printed with 84 mm distance between their feed lines, whereas one patch will be used for transmission, and the other will be used for reception. The distance between these two patches is optimized for achieving more than −50 dB isolation throughout the band of operation. Microstrip line feeding technique with inset feeding is used here for greater impedance matching. DGS is printed in the bottom layer. DGS is used to obtain a better isolation level as it is placed between two patches. This antenna is designed and simulated using ANSYS HFSS. Optimized

parameters for patch and DGS are given in Table 1. In Figure 1, the trimetric view, side view, top view, and bottom view with detailed parameter marking of the proposed antenna are shown. Figure 2 shows the simulated S-parameters of the proposed antenna. It can be depicted from the figure that the proposed antenna has -10 dB impedance bandwidth of 280 MHz (FBW = 4.8%) and a low mutual coupling reaching -85 dB at the center frequency.

Table 1. Optimized parameters for the top and bottom layer designs of the proposed antenna.

Parameter	Value, mm	Parameter	Value, mm
$F1$	18.5	$L1$	10
$F2$	4	$L2$	2
$F3$	10.2	$L3$	4
$F4$	15.2	$L4$	4.75
$F5$	34	$L5$	8.5
$F6$	2.6	$W1$	15
$H1$	12.93	$W2$	6.2
$H2$	5	$W3$	4
$H3$	22.5	$W4$	28
$H4$	12.5	$W5$	46.3
$H5$	5	$G1$	2
$G2$	2.4	$G3$	2

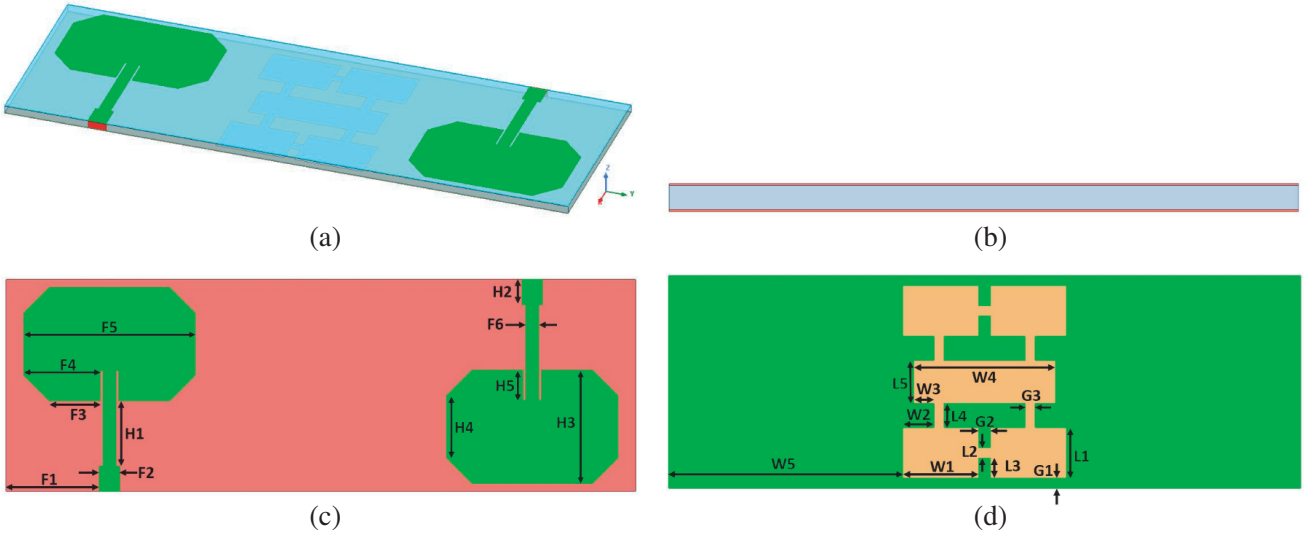

Figure 1. Proposed full-duplex patch antenna. (a) Trimetric view. (b) Side view. (c) Top view with detailed parameter marking. (d) Bottom view with detailed parameter marking.

2.2. Patch Design Steps

The evolution of the proposed antenna is shown in Figure 3. Firstly, patches of the top layer are designed only as simple rectangular patches. Simple rectangular patches have shown a bandwidth of 190 MHz from 5.26 GHz to 5.45 GHz. However, it does not have any bandwidth under -50 dB for the S_{21} parameter. Secondly, a corner cut in all four corners of both patches with the same size is

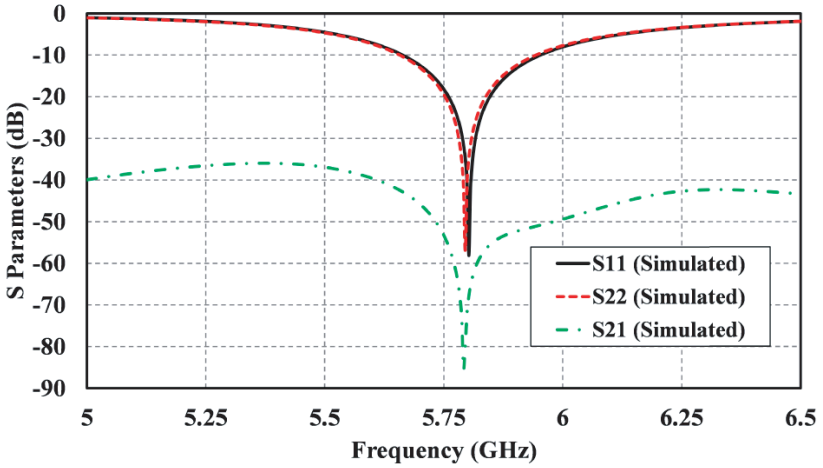

Figure 2. Simulated S parameters of the proposed antenna.

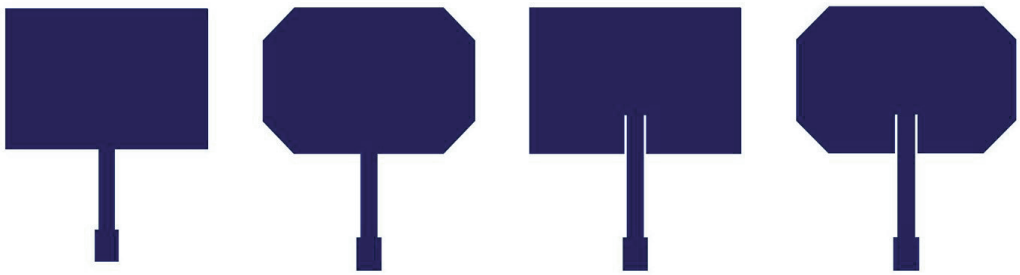

Figure 3. Evolution of the patch of the proposed antenna.

introduced. After that, the antenna has resonance shifted to the right with a bandwidth of 130 MHz from 5.55 GHz to 5.68 GHz. Also, an isolation bandwidth of 150 MHz from 5.77 GHz to 5.92 GHz under −50 dB is obtained. However, this bandwidth under −50 dB is not workable because it is not in the range where the patch antenna works. After that, only inset feeding is introduced, which has increased impedance matching bandwidth to 220 MHz from 5.36 GHz to 5.58 GHz. In this case, a bandwidth of 200 MHz from 5.47 GHz to 5.67 GHz has been found under −50 dB for the S_{21} parameter. Moreover, this case shows a portion of bandwidth from 5.47 GHz to 5.58 GHz, which is workable. Finally, after combining the corner cut and inset feeding cases, a bandwidth of 280 MHz from 5.67 GHz to 5.95 GHz for the S_{11} parameter and a bandwidth of 250 MHz from 5.73 GHz to 5.98 GHz for the S_{21} parameter are achieved. Design steps are compared for S_{11} and S_{21} parameters, which are given in Figure 4 and Figure 5, respectively.

2.3. Impact of DGS

DGS is particularly useful for implementing cross polarization suppression [24], higher order harmonics reduction [25], bandwidth enhancement [26], isolation improvement [27], and for improving radiation properties [28]. Different shapes like dumbbell, open arrowhead, spiral head, "H" shape, "U" shape, vertically periodic, and horizontally periodic are already proposed for these purposes for microstrip patch antenna as it also offers integration without any spacing or circuit modeling complexity [29]. DGS causes the disturbance in surface current distribution that ultimately results in increased effective inductance and capacitance.

A closed rectangular loop with rectangles in corners is designed in the proposed DGS. Another rectangle is placed in the middle, which is also connected to the loop. The structure is placed in between two patches. A difference is recorded in the S_{21} parameter after introducing the DGS, which is

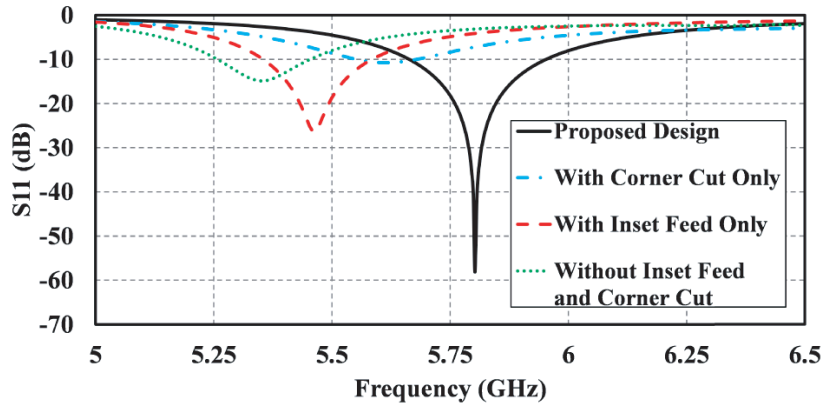

Figure 4. Simulated S_{11} parameters for different patch design steps.

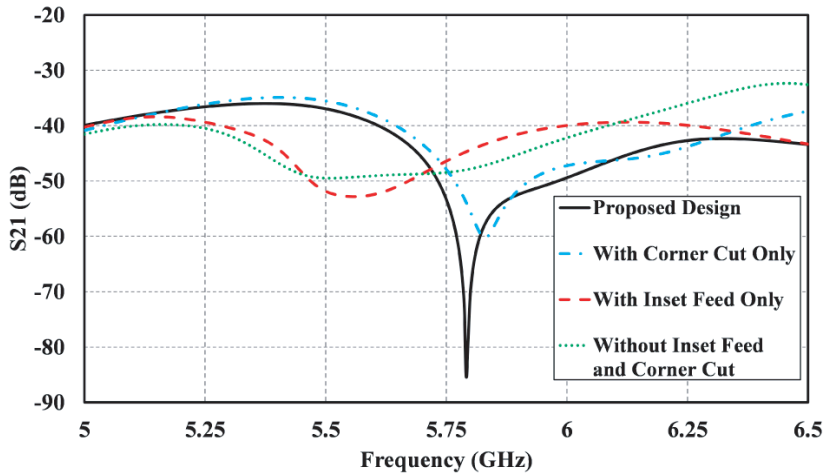

Figure 5. Simulated S_{21} parameters for different patch design steps.

shown in Figure 6. Without DGS, S_{21} has a bandwidth of 80 MHz from 5.79 GHz to 5.87 GHz, whereas the bandwidth is 250 MHz with DGS. Also, the minimum S_{21} is -50.65 dB and -85 dB without DGS and with DGS, respectively. In Figure 7, it is shown that surface currents are accumulated around DGS, which reduces the mutual coupling between TX and RX ports. It proves the impact of DGS in isolation improvement. This simulation is done at 5.8 GHz.

2.4. Impact of Inserting Foam in between

Another important feature of the proposed design is of using foam between the top and bottom PET paper layers. A low loss, flexible foam is used for this purpose. The reason for using foam in between is to provide better structural stability and bandwidth improvement. The foam layer and PET paper layers are attached using glue in between. In Figure 8, simulated S parameters are compared by placing foam and air between PET paper layers. S_{11} parameters have shifted when the foam is used instead of air. For air, bandwidth is around 290 MHz from 5.78 GHz to 6.07 GHz, whereas for foam bandwidth is around 280 MHz from 5.67 GHz to 5.95 GHz. Also, S_{21} is not under 50 dB for any frequency range when air is between PET paper layers, whereas S_{21} has a bandwidth of 250 MHz from 5.73 GHz to 5.98 GHz when the foam is used. Also, the antenna is examined without any gap in between by placing two PET paper layers together. As expected, it shifts the resonant frequency at 5.34 GHz with a smaller bandwidth of 95 MHz. The resonant frequency is reduced as effective permittivity is increased due to

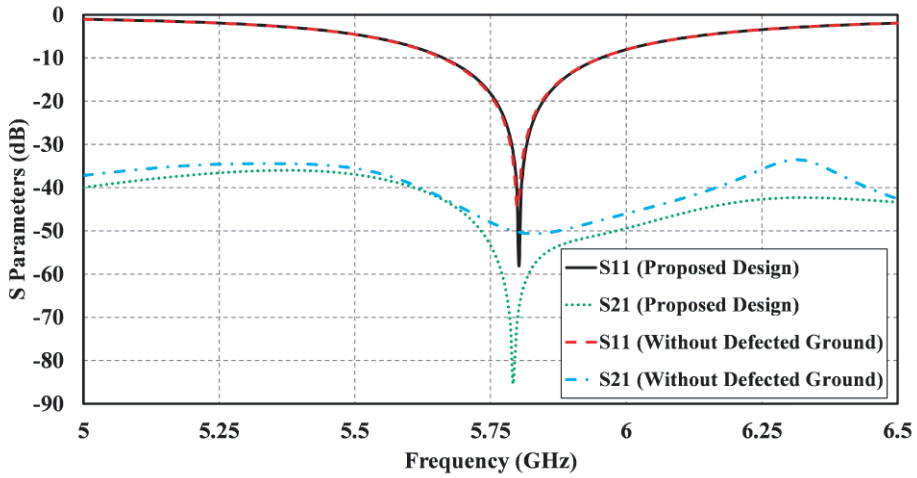

Figure 6. Simulated S parameters comparison of the antenna with and without DGS.

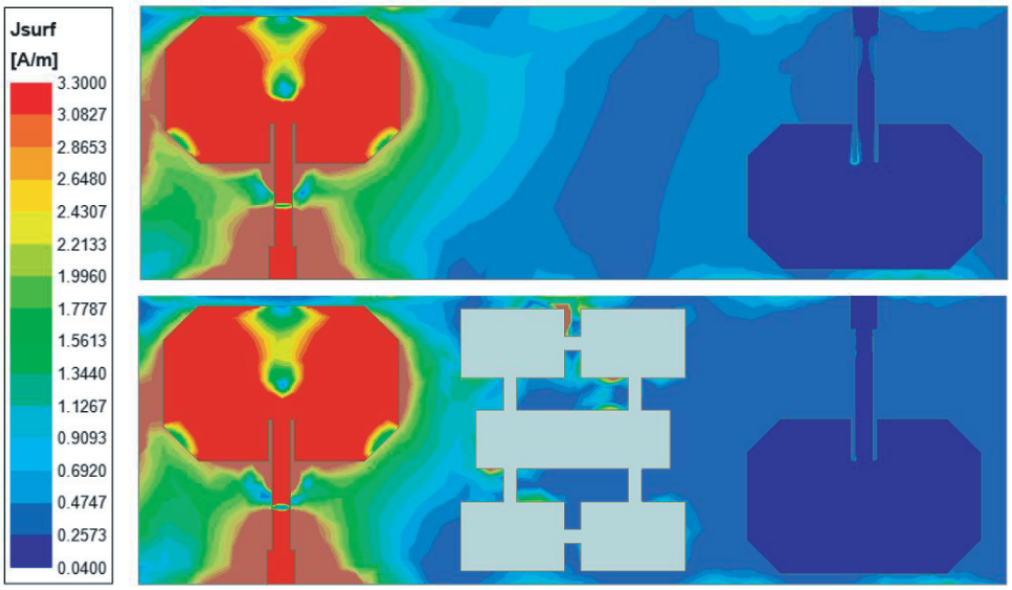

Figure 7. Simulated surface current density comparison of the antenna without and with DGS at 5.8 GHz.

the removal of the foam layer. Therefore, the foam has important contributions to obtaining desired antenna parameters.

2.5. Human Phantom Loading

As this antenna has the option to be used as a wearable one, antenna performance needs to be investigated when it is loaded with human tissue. A tissue mimicking phantom model is created by placing layers of muscle, fat, and skin on top of each other, respectively, as shown in Figure 9(a). The electrical properties of these layers can be found using Debye equation which can be expressed as [30],

$$\epsilon_\tau = \epsilon_\infty + \frac{\epsilon_s - \epsilon_\infty}{1 + j\omega\tau} - j\frac{\sigma_s}{\omega\epsilon_o}, \tag{1}$$

Here, "ϵ_τ" refers to complex permittivity; "ϵ_∞" refers to optical permittivity; "ϵ_s" refers to static permittivity; "ω" is the angular frequency; "τ" is the relaxation time; "σ_s" is the conductivity; and

Table 2. Properties of skin, fat and muscle layer at 5.8 GHz [31].

Tissue	Permittivity	Conductivity, S/m	Density, kg/m^3	Loss tangent
Skin	35.114	3.717	1090	0.418
Fat	4.9549	0.29313	1150	0.186
Muscle	48.485	4.9615	1050	0.342

"ϵ_o" is free space permittivity. In Table 2, the electrical properties of the layer, which are found in (1), are listed for 5.8 GHz frequency. The permittivity of the skin and muscle layers is high as they have more water content present and has a significant influence on the electric field.

To simulate the effect of human phantom loading, the proposed antenna is placed over a human phantom structure consisting of skin, fat, and muscle layers. The size of the phantom structure is $70 \times 150\,\text{mm}^2$. The skin, fat, and muscle layer heights are 2 mm, 5 mm, and 20 mm, respectively. In Figure 10(a), the S_{11} parameter for different gap distances between the antenna and phantom is analyzed. A small amount of shifting in resonant frequency is observed from 5.77 GHz to 5.82 GHz, while the gap between the antenna and phantom is increased from 0 mm to 2 mm. This is expected since the DGS is between the antennas, and it does not overlap with antenna elements. The proposed configuration leads to a directional radiation pattern which minimizes any effects on the resonant

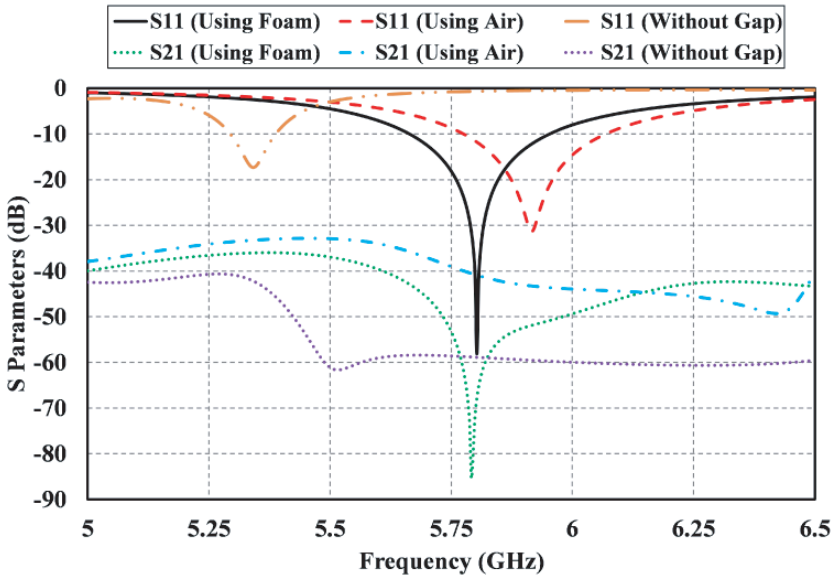

Figure 8. Simulated S parameters comparison for foam and air in between top and bottom PET paper layers.

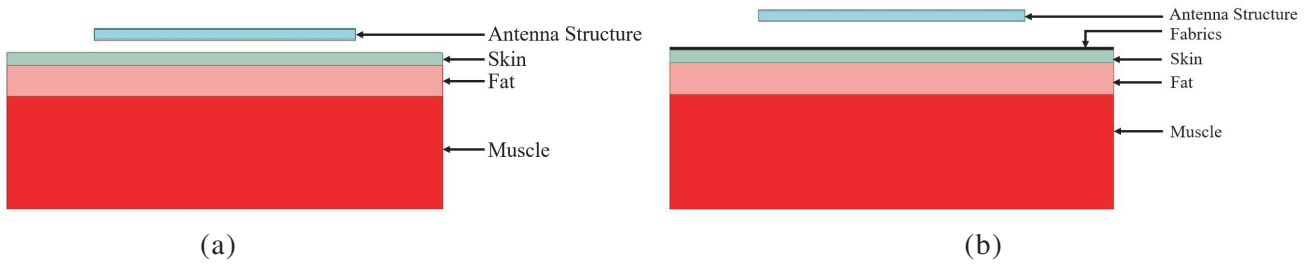

Figure 9. Side view of the antenna over the phantom model (a) without fabrics, (b) with fabrics.

frequency changes. Similarly, in Figure 10(b), the S_{21} parameter of the antenna is analyzed. For 0 mm and 1 mm gap distance, isolation was below −50 dB in 5.8 GHz, while it went down to −47 dB for 2 mm gap distance due to the distraction of electric field distribution by the electrical properties of the phantom layer.

To analyze the impact of clothing on antenna performance, a fabric layer is also added over the skin layer, as seen in Figure 9(b). The antenna is simulated with two different fabrics (fleece and leather). The permittivity of the fleece and leather layer is 1.17 and 2.95, along with loss tangents of 0.0035 and 0.006, respectively [32]. The fleece and leather layers have thicknesses of 0.05 mm and 0.5 mm, which are

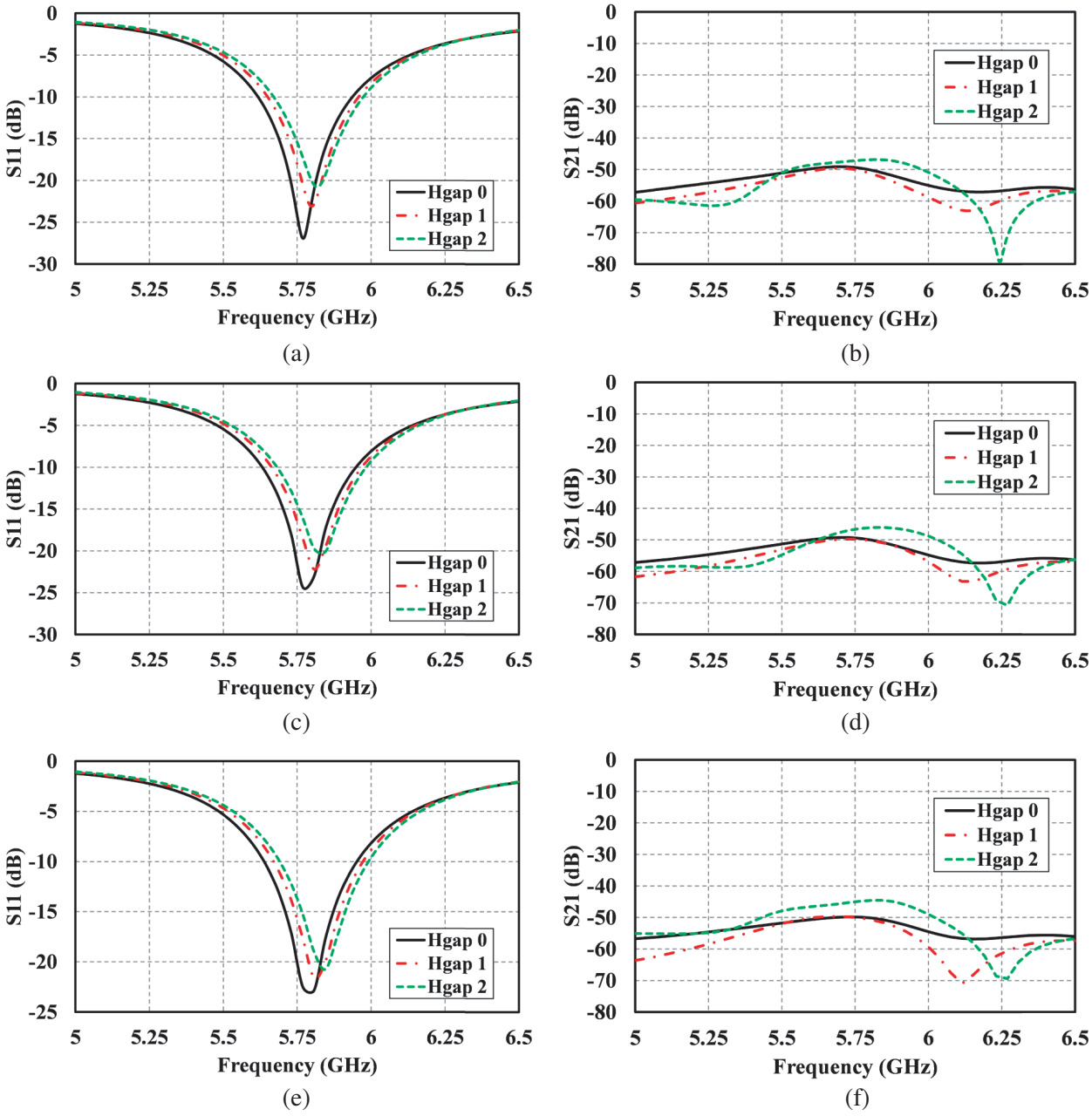

Figure 10. Simulated (a) S_{11} parameter, (b) S_{21} parameter directly over skin, (c) S_{11} parameter, (d) S_{21} parameter over fleece fabrics, (e) S_{11} parameter, (f) S_{21} parameter over leather fabrics comparison for different positions of the antenna over the phantom model.

the conventional thickness for these fabrics. Figures 10(c)–10(f) show S parameters when the antenna is simulated over the phantom model with fabric layers. As seen, S_{11} and S_{21} show similar patterns even after applying these two different kinds of fabrics. Therefore, it can be remarked that S parameters are not affected significantly due to human phantom loading even after placing over textile materials.

2.6. Specific Absorption Rate (SAR) Analysis

As the proposed antenna can be used for wearable applications, radiated electromagnetic energy must be kept under the limit of health hazards. SAR values are used as the parameter to ensure the safe usage of wearable antennas. The value of SAR can be calculated from the equation below:

$$SAR = \frac{\sigma |E|^2}{\rho} \tag{2}$$

where σ is the conductivity of the tissue in S/m, and ρ is the mass density of the tissue in kg/m^3. According to IEEE C95.1-2019 standard, SAR value should be under 1.6 W/kg averaged over 1 g tissue for partially body exposure [19, 31, 33–36]. To evaluate SAR, an input power of 100 mW is applied to both ports. The antenna is set on top of the phantom described in the previous section.

In Figure 11(a), the distribution of the SAR field over the antenna is demonstrated. The electric field is mostly accumulated in the region of the ports and patches as expected. In Figure 11(b), the average SAR is shown varying the gap between the antenna and human phantom. SAR value touches the 1.6 W/kg constraints when the gap is 0 mm. However, the value sharply decreases when the gap is introduced. At 1 mm and 2 mm gap, the average value of SAR is 0.9678 W/kg and 0.8549 W/kg, respectively. The value keeps itself around 0.8 W/kg if the gap distance continues to increase, which fulfills the condition of safe wearable use of the antenna. Moreover, as previously stated, SAR value is determined over fleece and leather fabrics. At 0 mm gap, the SAR value is slightly over our constraint (1.7715 W/kg) for fleece. However, it drastically decreases to 1.0231 W/kg after increasing the gap to 1 mm and decreases further as the gap increases. For leather, the SAR value is well below the constraint for any gap value (1.4898 W/kg for 0 mm). Therefore, the antenna is also safe for the usage over clothing.

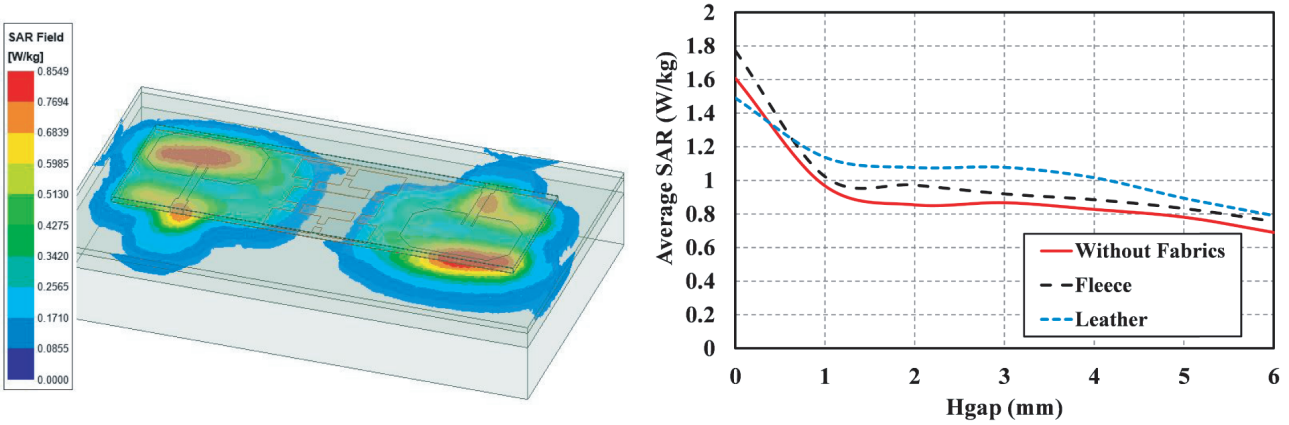

(a) (b)

Figure 11. (a) Simulated 1 g averaged SAR in the tissue with a gap of 2 mm between antenna and phantom. (b) Simulated average SAR with respect to the gap of antenna and phantom (Hgap).

2.7. Radiation Efficiency and Gain Analysis

Figure 12 shows the peak gain and radiation efficiency of the antenna with and without contact with the human phantom. The peak gain of the antenna at 5.8 GHz is 9.22 dB while maintaining over 9 dB in the whole 5.73 GHz to 5.95 GHz. When the antenna is placed 2 mm over the human phantom, the peak gain is increased to around 11 dB. This increase in gain happens because of the reflection of radiated waves

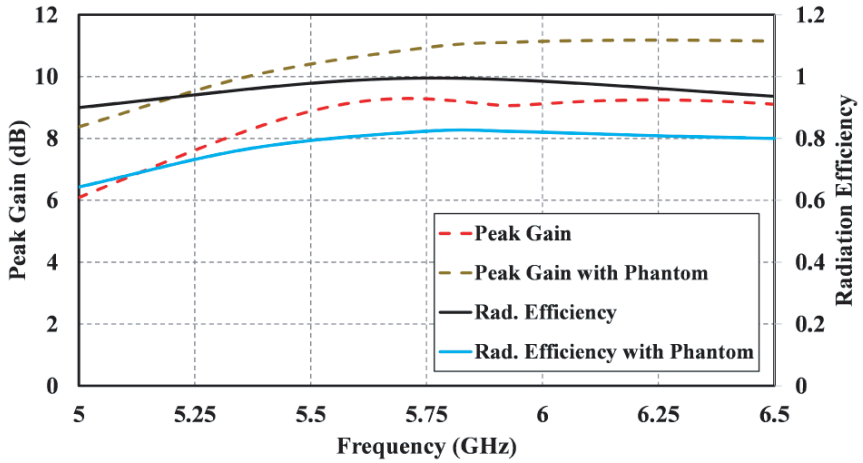

Figure 12. Peak gain and radiation efficiency of the proposed antenna.

from the human phantom as it is placed in close proximity (at around 0.04λ) [32]. Radiation efficiency is over 90% over the whole 5 GHz to 6.5 GHz bandwidth with 92.2% at 5.8 GHz. However, it decreases to 82% at 5.8 GHz while the antenna is put over the phantom due to the highly lossy characteristics of the phantom.

3. RESULTS AND DISCUSSION

This antenna is fabricated using a Fujifilm Dimatrix 2831 inkjet printer (DMP), which uses a 10 pL cartridge having 16 nozzles with each having diameter of 21 µm. These nozzles are operated based on the deformation of a piezoelectric material which is placed as the wall of the ink channel. Silver nanoparticle ink from Novacentrix is used. The printed antenna is sintered on the hotplate using 120°C temperature to generate constant conductivity over the whole printed area. After printing the top and bottom layers, "3M Super 77 Multipurpose Adhesive" is used to attach them to the foam layer. SMA ports are connected using the conductive soldering gel, and hot air is blown over the connecting region to ensure connectivity. The fabricated antenna is tested using Keysight Fieldfox N9952A microwave analyzer. Figure 13 shows some steps of fabrication and characterization of the proposed antenna.

Figure 14 shows the comparison of S_{11}, S_{21}, and S_{22} parameters of the proposed antenna. S_{11} and S_{22} parameters work under −10 dB in the proposed bandwidth for the fabricated antenna. Measurement shows a slightly wider bandwidth than the simulation. The differences between the experiment and simulation are attributed to the imperfection of the fabrication due to the uneven ink layer distribution by the inkjet printer. Considering the presence of losses, the bandwidth is also calculated based on −20 dB return loss. As seen, the proposed antenna has simulated and measured −20 dB bandwidths of 80 MHz (FBW = 1.38%) and 220 MHz (FBW = 3.79%), respectively. The antenna has a measured isolation below −40 dB from 5.18 GHz to 6.45 GHz. The isolation is less than −50 dB throughout the band of interest. Note that all mutual coupling measurements are conducted in a highly reflective laboratory to take into account environmental reflections. The differences between simulated and measured isolations are attributed to reflections from the ambient environment. Furthermore, the coaxial cables used during the measurements degrade the symmetricity and may cause more self interference than expected.

Figure 15 shows the placement of antenna over the curved surface for bending tests, which are performed in two directions. The bending radius for this experiment is 5 cm. For diagonal bending case, antenna is placed exactly at 45°. Measured S-parameters of the bent antenna are given in Figure 16. S_{11} is under −10 dB for both parallel and diagonal bendings from 5.6 GHz to 6.04 GHz, which is similar to the unbent case. However, resonant frequency shifts to 5.9 GHz, which is due to a change in effective permittivity as it was placed over a paper towel roll during measurement. The S_{21} parameter is under −50 dB for the whole bandwidth. Hence, the antenna maintains a robust

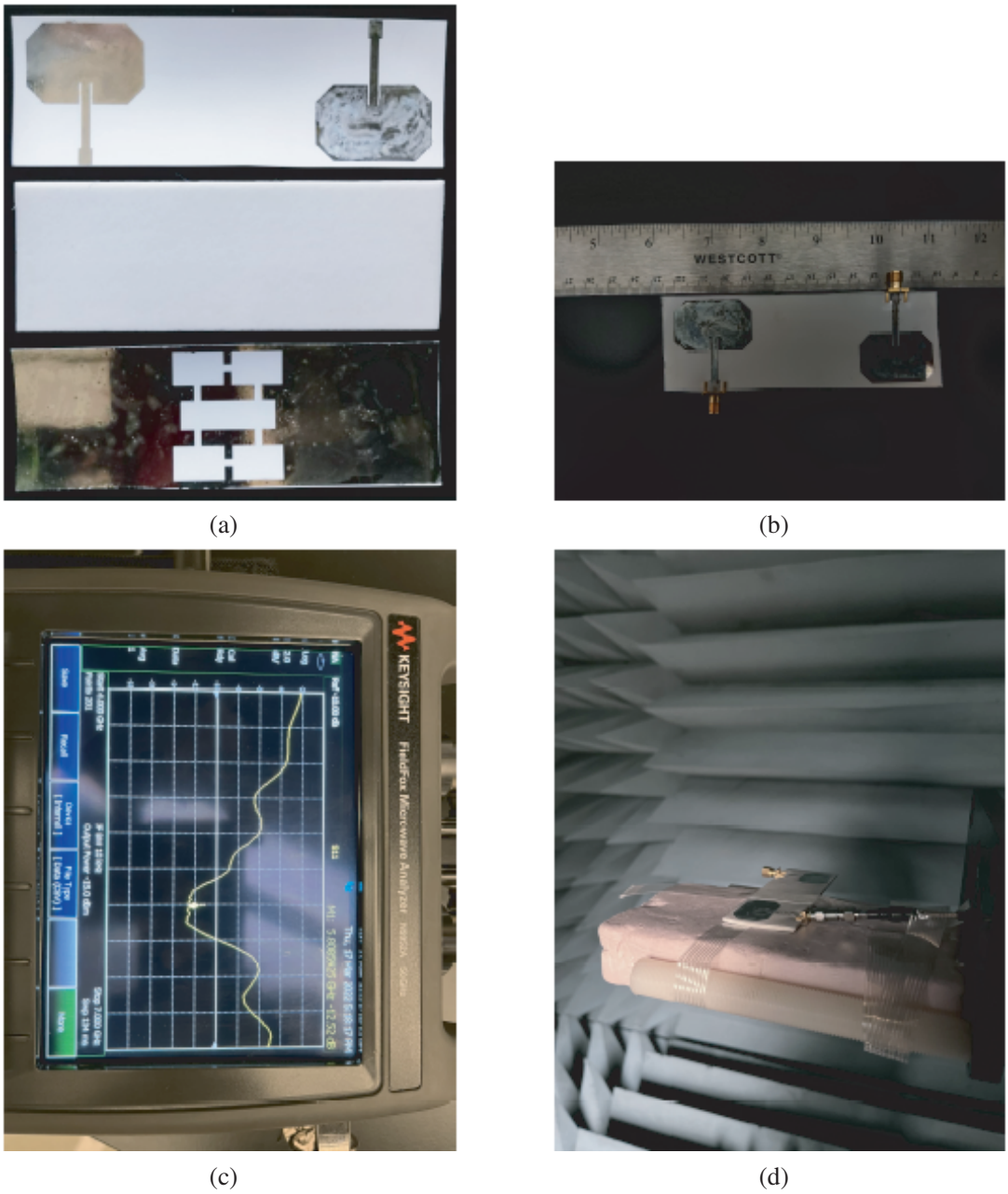

(a) (b)

(c) (d)

Figure 13. Images of fabricated antenna. (a) Top layer, foam and bottom layer. (b) Glued and soldered final version. (c) Testing with network analyzer. (d) Antenna in the anechoic chamber.

performance in desired bandwidth.

To assess and characterize antenna performance for on body applications, the antenna is placed over different body parts like the belly and arm (see Figure 17). As shown in Figure 18, there is a slight shift in the resonant frequency (around 5.65 GHz) compared to free space measurement. However, it maintains S_{11} below -10 dB at 5.8 GHz while maintaining -50 dB isolation simultaneously. These measurements demonstrate that the proposed antenna is robust in human loading conditions.

In Figure 19, normalized co-polarized and cross-polarized E and H plane patterns for the simulated and measured cases at 5.8 GHz are shown. The antenna is measured by exciting one port and terminating the other port with a 50 Ω load. It is shown that the measured and simulated patterns match very well for

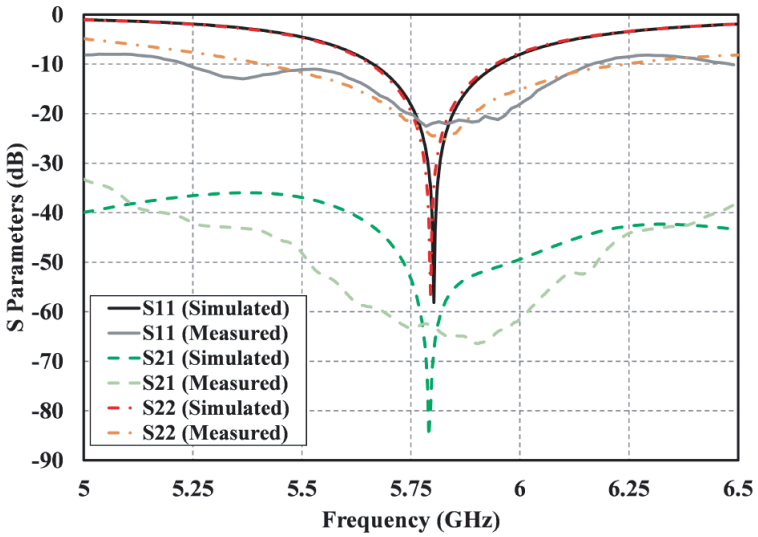

Figure 14. Measured and simulated S parameters of the proposed antenna.

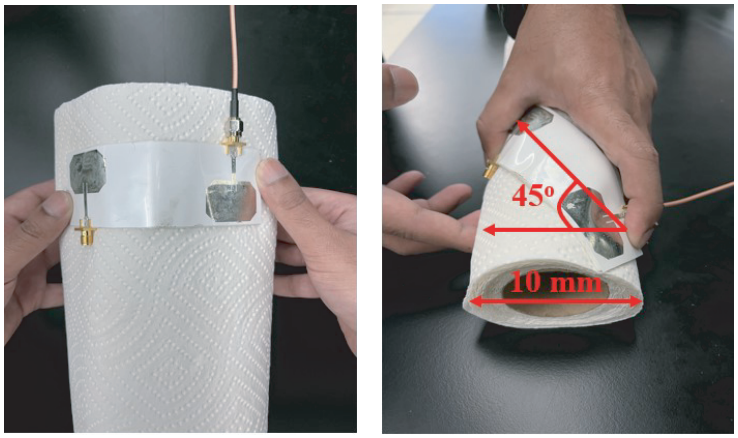

(a) (b)

Figure 15. Antenna is bent (a) parallelly to the patch, (b) diagonally to the patch.

both cases, with minor discrepancies due to measurement tolerance. The antenna shows unidirectional characteristics in the boresight with a very low amount of radiation in the back lobe. The antenna also has a measured front-to-back-ratio (FBR) of 10 dB. The calculated and measured values are consistent with side lobe levels of some full-duplex and MIMO antennas from the literature [37–40]. Co- and cross-polarized planes maintain a difference of 20 dB in the boresight direction for both planes. In Table 3, the proposed antenna is compared with previously reported full-duplex antennas from the literature. As seen, the current design differs from recent full-duplex antennas by achieving the largest isolation level in addition to being flexible for wearable applications. Also, the design has comparable bandwidth and peak gain with the literature. Please note that the majority of antennas introduced are on rigid substrates (i.e., [2, 3, 22, 37]) and are not suitable for conformal full-duplex applications. Compared to recent flexible full-duplex implementations [19–21, 38], the proposed antenna has much higher isolation (< -50 dB) in the band of interest. From Table 3, it is seen that the highest isolation measured so far for flexible antennas is -20 dB. These designs will need to cancel an additional -30 dB for the use in a full-duplex system. The extra burden on analog and digital cancellation circuits will increase the cost and complexity of the overall system. While [21], which has the same center frequency, reports a higher bandwidth, the proposed design has higher measured isolation between transmitting and receiving ports

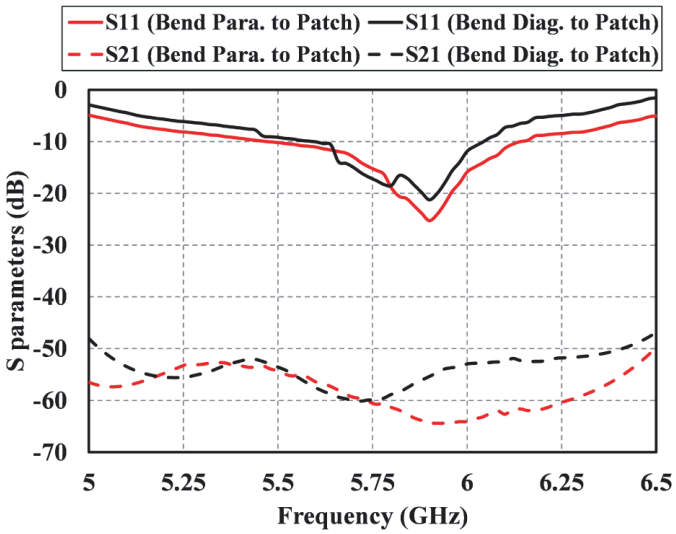

Figure 16. Measured effect of bending on S parameters of the proposed antenna.

(a) (b)

Figure 17. Proposed antenna tested on different parts of the body. (a) Belly. (b) Arm.

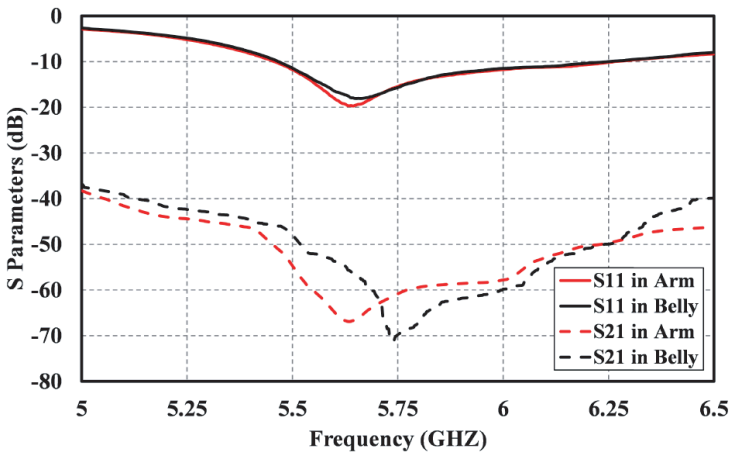

Figure 18. Measured S parameters for on body characterization.

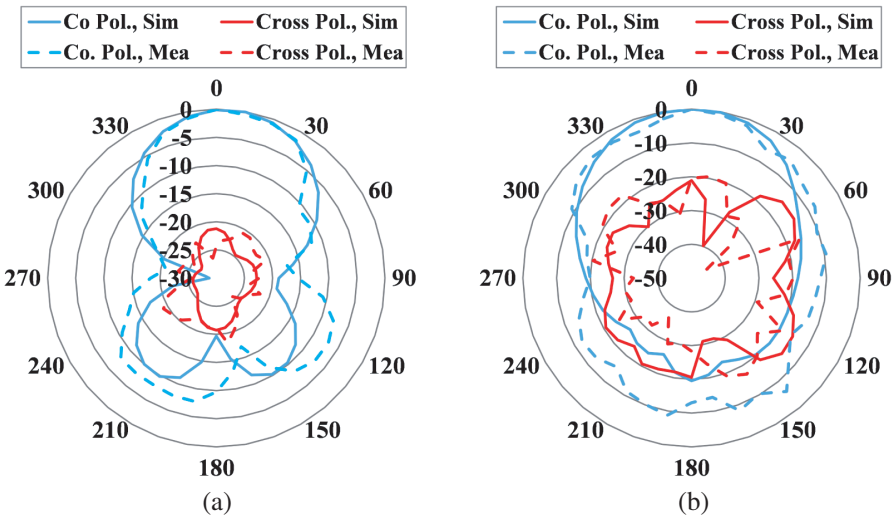

Figure 19. Normalized simulated and measured radiation pattern of (a) E plane and (b) H plane at 5.8 GHz.

Table 3. Comparison of proposed antenna with previously proposed full-duplex works.

Reference	Resonant frequency, GHz	Fractional bandwidth	Isolation, dB	Peak gain, dB	Flexibility	Dimensions
[2]	2.4	5%	≤ -35	4	No	$0.68\lambda \times 0.496\lambda \times 0.012\lambda$
[3]	4.75–5.18	8.66%	≤ -50	11	No	$3.04\lambda \times 0.99\lambda \times 0.075\lambda$
[19]	2.4	4.8%	≤ -20	7.5	Yes	-
[20]	2.4	4.2%	≤ -15	8.4/2.5	Yes	-
[21]	5.8	6.9%	≤ -20	4/6	Yes	$4.64\lambda \times 0.77\lambda \times 0.046\lambda$
[22]	4.9, 5.8	4.08%, 4.65%	≤ -29.8	5.75, 6.49	No	$\lambda \times 1.22\lambda \times .33\lambda$
[37]	3.3	2.4%	≤ -36	4.3	No	$0.56\lambda \times 0.56\lambda \times 0.0017\lambda$
[38]	2.4	3.67%	≤ -15	4.2	Yes	$3.14\lambda \times 0.23\lambda \times 0.026\lambda$
Proposed work	**5.8**	**4.8%**	$\mathbf{\leq -50}$	**9.22**	**Yes**	$\mathbf{2.41\lambda \times 0.81\lambda \times 0.036\lambda}$

and smaller size. Furthermore, although the antenna designs of [2] and [37] have smaller sizes, these designs do not have flexibility, and they demonstrate lower measured isolation levels. Similarly, [3] has a high fractional bandwidth at the expense of a larger size.

4. CONCLUSION

In this article, a flexible full-duplex antenna on PET paper is proposed for 5.8 GHz wearable applications. Inset feeding and corner cut along with DGS are introduced to implement -50 dB isolation on the resonant frequency with around 220 MHz bandwidth. The antenna can be fabricated easily using inkjet printing on PET paper which is glued with a foam layer afterward. Bending tests and on body characterization are performed on the fabricated antenna. Antenna shows desired performance in all the experiments making it a robust performer. It also provides high gain, high radiation efficiency, and low SAR level, making it a suitable candidate for full-duplex wearable applications.

ACKNOWLEDGMENT

Authors would like to thank PulseLarsen Antennas for providing the necessary setup in anechoic chamber to measure antenna parameters. Authors also like to thank National Science Foundation (NSF) for supporting this work under Grant No. ECCS-2104513.

REFERENCES

1. Sabharwal, A., P. Schniter, D. Guo, D. W. Bliss, S. Rangarajan, and R. Wichman, "In-band full-duplex wireless: Challenges and opportunities," *IEEE Journal on Selected Areas in Communications*, Vol. 32, No. 9, 1637–1652, 2014.
2. Makar, G., N. Tran, and T. Karacolak, "A high-isolation monopole array with ring hybrid feeding structure for in-band full-duplex systems," *IEEE Antennas and Wireless Propagation Letters*, Vol. 16, 356–359, 2017.
3. Zhang, Y. M., S. Zhang, J. L. Li, and G. F. Pedersen, "A dual-polarized linear antenna array with improved isolation using a slotline-based 180° hybrid for full-duplex applications," *IEEE Antennas and Wireless Propagation Letters*, Vol. 18, No. 2, 348–352, 2019.
4. Ta, S. X., N. Nguyen-Trong, V. C. Nguyen, K. K. Nguyen, and C. Dao-Ngoc, "Broadband dual-polarized antenna using metasurface for full-duplex applications," *IEEE Antennas and Wireless Propagation Letters*, Vol. 20, No. 2, 254–258, 2021.
5. Kirtania, S. G., A. W. Elger, M. Hasan, A. Wisniewska, T. Karacolak, and P. K. Sekhar, "Flexible antennas: A review," *Micromachines*, Vol. 11, No. 9, 847, 2020.
6. Memon, A. W., I. L. de Paula, B. Malengier, S. Vasile, P. Van Torre, and L. Van Langenhove, "Breathable textile rectangular ring microstrip patch antenna at 2.45 GHz for wearable applications," *Sensors*, Vol. 21, No. 5, 1635, 2021.
7. Ahmed, M. I., M. F. Ahmed, and A. H. A. Shaalan, "Novel electro-textile patch antenna on jeans substrate for wearable applications," *Progress In Electromagnetics Research C*, Vol. 83, 255–265, 2018.
8. Nikbakhtnasrabadi, F., H. El Matbouly, M. Ntagios, and R. Dahiya, "Textile-based stretchable microstrip antenna with intrinsic strain sensing," *ACS Applied Electronic Materials*, Vol. 3, No. 5, 2233–2246, 2021.
9. Kirtania, S. G., B. A. Younes, A. R. Hossain, T. Karacolak, and P. K. Sekhar, "CPW-fed flexible ultra-wideband antenna for IoT applications," *Micromachines*, Vol. 12, No. 4, 453, 2021.
10. Farooqui, M. F. and A. Kishk, "3-D-printed tunable circularly polarized microstrip patch antenna," *IEEE Antennas and Wireless Propagation Letters*, Vol. 18, No. 7, 1429–1432, 2019.
11. Abutarboush, H. F., W. Li, and A. Shamim, "Flexible-screen-printed antenna with enhanced bandwidth by employing defected ground structure," *IEEE Antennas and Wireless Propagation Letters*, Vol. 19, No. 10, 1803–1807, 2020.
12. Tran, N. A., H. N. Tran, M. C. Dang, and E. Fribourg-Blanc, "Copper thin film for RFID UHF antenna on flexible substrate," *Advances in Natural Sciences: Nanoscience and Nanotechnology*, Vol. 1, No. 2, 025016, 2010.
13. El Maleky, O., F. B. Abdelouahab, M. Essaaidi, and M. A. Ennasar, "Design of simple printed dipole antenna on flexible substrate for UHF band," *Procedia Manufacturing*, Vol. 22, 428–435, 2018.
14. Chen, S. J., C. Fumeaux, B. Chivers, and R. Shepherd, "A 5.8-GHz flexible microstrip-fed slot antenna realized in PEDOT: PSS conductive polymer," *Proc. IEEE International Symposium on Antennas and Propagation (APSURSI)*, 1317–1318, June 2016.
15. Kadry, M., M. El Atrash, and M. A. Abdalla, "Design of an ultrathin compact flexible dual-band antenna for wearable applications," *Proc. IEEE International Symposium on Antennas and Propagation & USNC/URSI National Radio Science Meeting*, 1949–1950, July 2018.

16. Jalil, M., M. Rahim, N. Samsuri, N. Murad, N. Othman, and H. Majid, "On-body investigation of dual-band diamond textile antenna for wearable applications at 2.45 GHz and 5.8 GHz," *Proc. 7th European Conference on Antennas and Propagation (EuCAP)*, 414–417, April 2013.
17. Hamouda, Z., J. L. Wojkiewicz, A. A. Pud, L. Kone, S. Bergheul, and T. Lasri, "Flexible UWB organic antenna for wearable technologies application," *IET Microwaves, Antennas & Propagation*, Vol. 12, No. 2, 160–166, 2018.
18. Du, C. Z., K. J. Li, and S. S. Zhong, "A novel flexible hexagon wideband CPW-fed monopole antenna for UWB applications," *Microwave and Optical Technology Letters*, Vol. 63, No. 7, 1899–1905, 2021.
19. Mao, C. X., Y. Zhou, Y. Wu, H. Soewardiman, D. H. Werner, and J. S. Jur, "Low-profile strip-loaded textile antenna with enhanced bandwidth and isolation for full-duplex wearable applications," *IEEE Transactions on Antennas and Propagation*, Vol. 68, No. 9, 6527–6537, 2020.
20. Wagih, M., G. S. Hilton, A. S. Weddell, and S. Beeby, "Dual-polarized wearable antenna/rectenna for full-duplex and MIMO Simultaneous Wireless Information and Power Transfer (SWIPT)," *IEEE Open Journal of Antennas and Propagation*, Vol. 2, 844–857, 2021.
21. Mao, C. X., D. Vital, D. H. Werner, Y. Wu, and S. Bhardwaj, "Dual-polarized embroidered textile armband antenna array with omnidirectional radiation for on-/off-body wearable applications," *IEEE Transactions on Antennas and Propagation*, Vol. 68, No. 4, 2575–2584, 2020.
22. Mallat, N. K. and A. Iqbal, "Substrate integrated waveguide-based simultaneous transmit and receive antenna for full-duplex wearable devices," *International Journal of RF and Microwave Computer-aided Engineering*, e23188, 2022.
23. Hossain, A. R., A. A. Mertvyy, N. Tran, and T. Karacolak, "A high gain flexible antenna for full duplex system at 5.8 GHz with defected ground structure," *Proc. IEEE International Symposium on Antennas and Propagation and USNC-URSI Radio Science Meeting (AP-S/URSI)*, 1040–1041, July 2022.
24. Guha, D., M. Biswas, and Y. M. Antar, "Microstrip patch antenna with defected ground structure for cross polarization suppression," *IEEE Antennas and Wireless Propagation Letters*, Vol. 4, 455–458, 2005.
25. Sung, Y., M. Kim, and Y. S. Kim, "Harmonics reduction with defected ground structure for a microstrip patch antenna," *IEEE Antennas and Wireless Propagation Letters*, Vol. 2, 111–113, 2003.
26. Chiang, K. H. and K. W. Tam, "Microstrip monopole antenna with enhanced bandwidth using defected ground structure," *IEEE Antennas and Wireless Propagation Letters*, Vol. 7, 532–535, 2008.
27. Chung, Y., S. S. Jeon, D. Ahn, J. I. Choi, and T. Itoh, "High isolation dual-polarized patch antenna using integrated defected ground structure," *IEEE Microwave and Wireless Components Letters*, Vol. 14, No. 1, 4–6, 2004.
28. Kumar, C., M. I. Pasha, and D. Guha, "Defected ground structure integrated microstrip array antenna for improved radiation properties," *IEEE Antennas and Wireless Propagation Letters*, Vol. 16, 310–312, 2017.
29. Weng, L. H., Y. C. Guo, X. W. Shi, and X. Q. Chen, "An overview on defected ground structure," *Progress In Electromagnetics Research B*, Vol. 7, 173–189, 2008.
30. Doddipalli, S., A. Kothari, and P. Peshwe, "A low profile ultrawide band monopole antenna for wearable applications," *International Journal of Antennas and Propagation*, Vol. 2017, Art. No. 7362431, 2017.
31. Yang, H., X. Liu, Y. Fan, and L. Xiong, "Dual-band textile antenna with dual circular polarizations using polarization rotation AMC for off-body communications," *IEEE Transactions on Antennas and Propagation*, Vol. 70, No. 6, 4189–4199, 2022.
32. Almohammed, B., A. Ismail, and A. Sali, "Electro-textile wearable antennas in wireless body area networks: Materials, antenna design, manufacturing techniques, and human body consideration — A review," *Textile Research Journal*, Vol. 91, No. 5–6, 646–663, 2021.

33. IEEE standards for safety levels with respect to human exposure to electric, magnetic, and electromagnetic fields, 0 Hz to 300 GHz, IEEE Std. C95. 1-2019, 2019.
34. Zu, H. R., B. Wu, Y. H. Zhang, Y. T. Zhao, R. G. Song, and D. P. He, "Circularly polarized wearable antenna with low profile and low specific absorption rate using highly conductive graphene film," *IEEE Antennas and Wireless Propagation Letters*, Vol. 19, No. 12, 2354–2358, 2020.
35. Jiang, Z. H., Z. Cui, T. Yue, Y. Zhu, and D. H. Werner, "Compact, highly efficient, and fully flexible circularly polarized antenna enabled by silver nanowires for wireless body-area networks," *IEEE Transactions on Biomedical Circuits and Systems*, Vol. 11, No. 4, 920–932, 2017.
36. Samanta, G. and D. Mitra, "Dual-band circular polarized flexible implantable antenna using reactive impedance substrate," *IEEE Transactions on Antennas and Propagation*, Vol. 67, No. 6, 4218–4223, 2019.
37. Hussein, A. H., H. H. Abdullah, M. A. Attia, and A. M. Abada, "S-band compact microstrip full-duplex Tx/Rx patch antenna with high isolation," *IEEE Antennas and Wireless Propagation Letters*, Vol. 18, No. 10, 2090–2094, 2019.
38. Wen, D., Y. Hao, M. O. Munoz, H. Wang, and H. Zhou, "A compact and low-profile MIMO antenna using a miniature circular high-impedance surface for wearable applications," *IEEE Transactions on Antennas and Propagation*, Vol. 66, No. 1, 96–104, 2018.
39. Jayant, S., G. Srivastava, and S. Kumar, "Quad-port UWB MIMO footwear antenna for wearable applications," *IEEE Transactions on Antennas and Propagation*, Vol. 70, No. 9, 7905–7913, 2022.
40. Wen, D., Y. Hao, H. Wang, and H. Zhou, "Design of a MIMO antenna with high isolation for smartwatch applications using the theory of characteristic modes," *IEEE Transactions on Antennas and Propagation*, Vol. 67, No. 3, 1437–1447, 2019.